# Crystal structure of the extracellular cholinesterase-like domain from neuroligin-2

Jesko Koehnke*, Xiangshu Jin*, Elaine C. Budreck[†‡], Shoshana Posy*[§¶], Peter Scheiffele[†‡], Barry Honig*[§¶‖], and Lawrence Shapiro*[,**††]

Departments of *Biochemistry and Molecular Biophysics, [†]Physiology and Cellular Biophysics, and [‡]Neuroscience, [§]Center for Computational Biology and Bioinformatics, [¶]Howard Hughes Medical Institute, and **Edward S. Harkness Eye Institute, Columbia University, New York, NY 10032

Contributed by Barry Honig, December 12, 2007 (sent for review November 27, 2007)

**Neuroligins (NLs) are catalytically inactive members of a family of cholinesterase-like transmembrane proteins that mediate cell adhesion at neuronal synapses. Postsynaptic neuroligins engage in $Ca^{2+}$-dependent transsynaptic interactions via their extracellular cholinesterase domain with presynaptic neurexins (NRXs). These interactions may be regulated by two short splice insertions (termed A and B) in the NL cholinesterase domain. Here, we present the 3.3-Å crystal structure of the ectodomain from NL2 containing splice insertion A (NL2A). The overall structure of NL2A resembles that of cholinesterases, but several structural features are unique to the NL proteins. First, structural elements surrounding the esterase active-site region differ significantly between active esterases and NL2A. On the opposite surface of the NL2A molecule, the positions of the A and B splice insertions identify a candidate NRX interaction site of the NL protein. Finally, sequence comparisons of NL isoforms allow for mapping the location of residues of previously identified mutations in NL3 and NL4 found in patients with autism spectrum disorders. Overall, the NL2 structure promises to provide a valuable model for dissecting NL isoform- and synapse-specific functions.**

acetylcholinesterase-like | neurexin

The mammalian central nervous system is characterized by an elaborate pattern of synaptic connectivity in which thousands of individual neurons interact in a highly coordinated fashion to generate functional neuronal networks. The specificity of wiring is thought to rely at least in part on transsynaptic adhesion molecules that selectively link synaptic partners. One adhesion system that might be involved in such interactions is the neuroligin–neurexin (NL-NRX) complex (1–3). The NL family consists of four highly homologous proteins (NL1, -2, -3, and -4) (4, 5). All NLs are type I transmembrane proteins consisting of a large extracellular domain with sequence homology to cholinesterases (ChE) and short extracellular stalk, transmembrane, and cytoplasmic domains. Postsynaptic NLs bind to presynaptic NRXs to form adhesive complexes that bridge the synaptic cleft (6). *In vitro* studies indicate that both NLs and NRXs are sufficient to organize functional pre- or postsynaptic membrane specializations (7–10), and *in vivo* studies support important roles for NRXs and NLs in the recruitment of pre- and postsynaptic ion channels, respectively.

Genetic association studies in cohorts of patients with autism spectrum disorders (ASDs) revealed sequence variations in the genes encoding NL3 and NL4, as well as NRX genes (11–14), suggesting that functional alterations in this synaptic adhesion complex might be linked to neurodevelopmental disorders. The majority of candidate disease-associated sequence variants in NLs map to the ChE-domain of the proteins. Moreover, the ChE-domain of NLs is required for NRX binding and for the synapse-organizing activity of NL proteins. Sequence comparisons reveal up to 28% sequence identity with catalytically active ChEs. This large group of enzymes is characterized by an $\alpha/\beta$-hydrolase fold, with a catalytic amino acid triad in the center of the enzyme at the base of a deep pocket accessible from the surface of the molecule. In addition to this active site, cholinesterases bind a second substrate molecule through a so-called peripheral anionic site (PAS), which is lined with charged amino acid residues (15). Although NLs and ChE share substantial sequence similarity and show apparently redundant function in some assays (16), swapping the ChE-domain of NL1 with that of AChE abolishes NRX binding of NL1 and results in a protein with dominant-negative function in cultured neurons (17, 18). Despite these differences, the analogy between NLs and ChE has enabled preliminary structural modeling based on sequence alignments (10). These structural models suggested an oligomeric assembly of NL proteins, which was confirmed by biochemical cross-linking studies and analytical ultracentrifugation (1, 10). Mutation of amino acids in the predicted dimerization interface resulted in a loss of NL function, suggesting a requirement for lateral NL-NL interactions for the recruitment of presynaptic components.

Within their ChE-domains, the NL1, -2, -3, and -4 isoforms exhibit nearly 70% amino acid identity. Nevertheless, the isoforms exhibit differential interactions with NRX protein isoforms and differential localization at neuronal synapses (19–21). Some of these distinct properties are determined by small alternative splice insertions at two sites within the ChE domain termed A and B. Whereas NL2 and NL 3 undergo alternative splicing only at the A site (17-aa insertion for NL2), NL1 can additionally be modified by inclusion or exclusion of a 9-aa insertion at site B. In cellular and biochemical assays, NL1 containing an insert at site B (NL1B) exhibits greatly reduced binding to some neurexin isoforms, whereas it retains binding affinity for others (3, 17, 22). Moreover, NL1B has reduced ability to recruit GABAergic presynaptic terminals in cultured hippocampal neurons as compared with NL1(−) or NL1A (23). The presence or absence of an insert at site A does not significantly affect binding of NL to neurexin variants tested thus far (22). However, in cultured hippocampal neurons, the NL A insert promotes the association of neuroligins at contacts with GABAergic axons and enhances the ability of NLs to cluster GABAergic versus glutamatergic presynaptic proteins (23). Thus, it appears that the A insert can regulate cellular functions of NL molecules, but the molecular mechanism is presently unknown. Taken together, biochemical and cell biological studies implicate alternative splice insertions of NL and NRX as

Author contributions: J.K. and X.J. contributed equally to this work; J.K., P.S., B.H., and L.S. designed research; J.K. performed research; S.P. contributed new reagents/analytic tools; X.J., B.H., and L.S. analyzed data; and J.K., E.C.B., P.S., B.H., and L.S. wrote the paper.

The authors declare no conflict of interest.

Data deposition: The atomic coordinates have been deposited in the Protein Data Bank, www.pdb.org (PDB ID code 3BL8).

[‖]To whom correspondence may be addressed. E-mail: bh6@columbia.edu.

[††]To whom correspondence may be addressed at: Department of Biochemistry and Molecular Biophysics, Columbia University, 630 West 168th Street, New York, NY 10032. E-mail: lss8@columbia.edu.

This article contains supporting information online at www.pnas.org/cgi/content/full/0711701105/DC1.

critical determinants modulating transsynaptic interactions. However, the molecular logic of how alternative splicing alters NL-NRX interactions and function at synapses has remained obscure.

To gain better insight into these questions, we have initiated studies to obtain crystal structures of several NL and NRX protein family members. Here, we report the 3.3-Å crystal structure of the mouse NL2 ectodomain containing the 17-residue splice insertion A (NL2A). The overall topology of NL2A is similar to that of ChE, comprising a dimer of protomers with a characteristic $\alpha/\beta$ hydrolase fold. However, the crystal structure also reveals several distinctions in the extracellular domain of NL2 as compared with AChE. These findings provide insights into structure–function relationships for NLs and should provide an important basis for the interpretation of functional studies of NL isoform- and synapse-specific behavior.

## Results

**Overall Structure of Mouse Neuroligin-2A.** NL2A is the primary NL isoform localized at GABAergic synapses and one of the few synaptic adhesion molecules known to be concentrated at these synapses. To obtain structural insight into how NL2A might mediate its function, we sought to obtain a high-resolution structure of the NL2 ectodomain containing the A insert. The ectodomain from mouse NL2A was expressed in HEK293 cells and purified to near homogeneity. NL2A eluted in size-exclusion chromatography experiments on Sephadex 200 at a volume corresponding to ≈130 kDa, indicating a tightly associated solution dimer. This recombinant protein, encompassing residues 42–610 [supporting information (SI) Fig. 5], formed crystals that belong to space group *C*2, with two biological dimers in the asymmetric unit. The structure was determined at 3.3-Å resolution by multiple isomorphous replacement with anomalous scattering aided by molecular replacement with the structure of human butyryl cholinesterase (BChE) (PDB entry 1P0I) used as the search model. SI Table 1 shows the data collection and refinement statistics. The refined model (PDB entry 3BL8) includes residues 42–158 and 174–610 in chain A; 42–150 and 174–608 in chain B; 42–150 and 176–610 in chain C; and 42–150, 175–557, and 563–610 in chain D. The structure of the NL2A dimer has an ellipsoidal shape with dimensions of approximately 45 Å × 70 Å × 135 Å. Similar to ChEs, each NL2A protomer adopts the $\alpha/\beta$ hydrolase fold and consists of a 12-stranded central curved $\beta$-sheet surrounded by 14 $\alpha$-helices (Fig. 1*A*). Fig. 2 shows a comparison of the extracellular domain structure of BChE superimposed on that determined for NL2A. The pairwise root mean square deviation (rmsd) for $\alpha$-carbons between the structures of mouse NL2A and human BChE (PDB entry 1P0I) is 1.32 Å for 416 $C^{\alpha}$ atom pairs. Secondary structure elements are conserved between the NL2A and the BChE structure, with the exception of one $3_{10}$ helix ($\alpha$20) that is only present in NL2A but not in cholinesterases, and two short helices ($\alpha$1 and $\alpha$17) that are present in cholinesterases but are absent in NL2A (Fig. 2). The primary sequence of NL2A includes three consensus N-glycosylation sites at positions 98, 136, and 522. In the crystal structure, one protomer from each dimer in the asymmetric unit exhibits unambiguous electron density for carbohydrate moieties at Asn-98 and Asn-136, suggesting that at least these two sites are modified in HEK293 cells.

**Dimerization Interface.** Experiments in cultured neurons have demonstrated that oligomerization of NLs is necessary for their ability to promote the recruitment of presynaptic proteins (10). In agreement with these studies and previous analytical ultracentrifugation experiments (22), crystallized NL2A is present in a dimeric form. The dimerization interface of NL2A is topologically identical to that of esterases, consisting of a four-helix bundle with two helices contributed by each monomer (Fig. 1*B*).

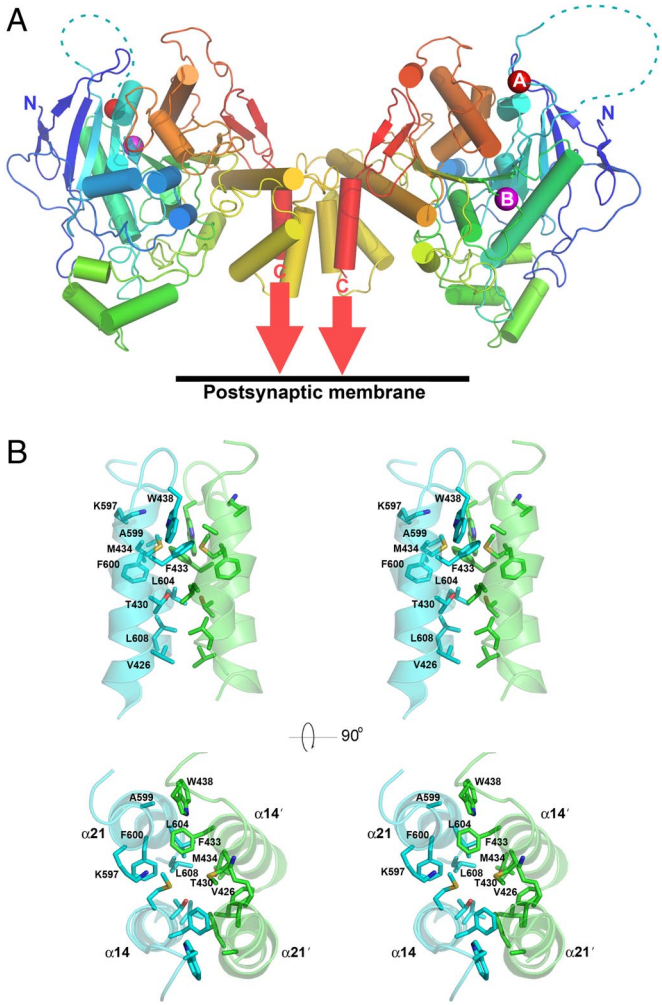


**Fig. 1.** Overall structure of NL2A dimer, and expanded view of the dimer interface. (*A*) Ribbon diagram of the NL2A dimer. Each protomer is represented in rainbow color running from N terminus (blue) to C terminus (red). The position of splice site A and the mapped position of splice site B are marked by red and magenta spheres, respectively. The majority of splice insertion A residues are disordered, and their connectivity is indicated by the dotted lines. N and C termini are indicated. (*B*) Dimer interface region, shown as stereo diagrams in two orthogonal views.

The dimerization interface contains an intricate network of hydrogen bond and salt bridge interactions, as well as hydrophobic contacts between residues within helices $\alpha$14 and $\alpha$21 from each monomer. Specifically, Arg-441 and Glu-429 make hydrogen bond and salt bridge interactions with Glu-603 and His-607 from the partner monomer, respectively. Hydrophobic contact pairs between residues from each monomer are Val-426–Leu-608; Thr-430–Leu-604; Phe-433–Met-434, Phe-600; and Trp-438–Ala-599. Previous studies demonstrated that alanine substitutions in the $\alpha$21-helix of NL1 in residues equivalent to Lys-597/Val-598 and Glu-603/Leu-604 resulted in decreased dimerization and higher-order oligomer formation of mutant NL1 (10). Notably, Glu-603, Leu-604, and Lys-597 directly participate in interactions across the dimer interface. Val-598 lies within the same $\alpha$21-helical bundle but contributes to the hydrophobic core of its own protomer. These data are consistent with site-directed mutagenesis results reported by Dean *et al.* (10) showing that NL function depends critically on these dimer interface residues. Interestingly, the residues that make intersubunit contacts across the dimer interface—Val-426, Phe-433,

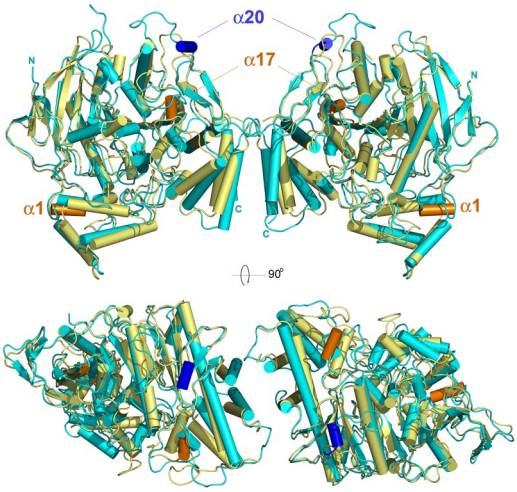


**Fig. 2.** Comparison of the secondary structure topologies of NL2A (cyan) and BChE (yellow). Helices present in NL2A but not in BChE are colored in dark blue; helices present in BChE but not in NL2A are colored in orange.

Met-434, Trp-438, Leu-604, and Leu-608—are entirely conserved across mammalian NL isoforms, with the exception of one substitution in NL3 (Val-426 to Thr). This suggests that all NL isoforms form dimers through the same interactions and that the dimerization interface might potentially support the formation of NL heterodimers. However, this remains to be tested experimentally.

**Occlusion of the Active Site.** Despite high sequence homology to ChEs, NLs are not catalytically active (10). This has been attributed to a glycine substitution of the active-site serine in all NL isoforms (4) (SI Fig. 5). However, whether NLs possess other structural features related to the esterase activity of AChE has not been determined. Cholinesterases are characterized by deep substrate binding pockets and a PAS (15). The structure of NL2A shows that the active-site pocket is completely occluded by an "omega loop" encompassing residues 107–141 (Fig. 3*A*). Superposition of the structure of NL2A with the structure of human AChE reveals that the omega loop containing the $\alpha$1-helix (Fig. 3*A*) occupies both the active site and PAS binding sites. A NL-specific disulfide bond (Cys-487–521) may enable the $\alpha$18–$\alpha$19 intervening loop to stabilize the omega loop inside the active-site gorge (Fig. 3*A*). This unique Cys-487–521 disulfide bridge is only conserved in vertebrate but not in invertebrate NLs (Fig. 4). In contrast, two additional disulfide bonds (Cys-106–141 and Cys-317–328) are highly conserved in cholinesterases and NLs.

**Structural Elements That Regulate NL-NRX Interactions.** Previous studies revealed two mechanisms for the regulation of NL-NRX interactions. (*i*) Incorporation of alternative splice insertions in the NL ectodomain regulates interaction with specific NRX isoforms, and (*ii*) NL-NRX binding requires the presence of calcium (2, 4). Putative $Ca^{2+}$ binding sites in NRX have been identified (24), but other studies provided evidence that NL is the calcium binding molecule (2). Modeling studies suggested that the capacity of NL to bind $Ca^{2+}$ might be based on two contiguous EF hand-like motifs beginning with residue 388 and ending at residue 474 (25). In NL2A, this region corresponds to helices $\alpha$12–$\alpha$16. The crystal structure reveals that the $\alpha$12–$\alpha$13 and $\alpha$14–$\alpha$15 intervening loops (Fig. 3*B*) both display sequences rich in Asp, Glu, and Asn residues, as is characteristic of EF hand motifs. However, despite the presence of 3 mM $CaCl_2$ in the crystallization medium, we do not observe electron density for calcium ions in the structure. Additionally, the NL2A EF hands

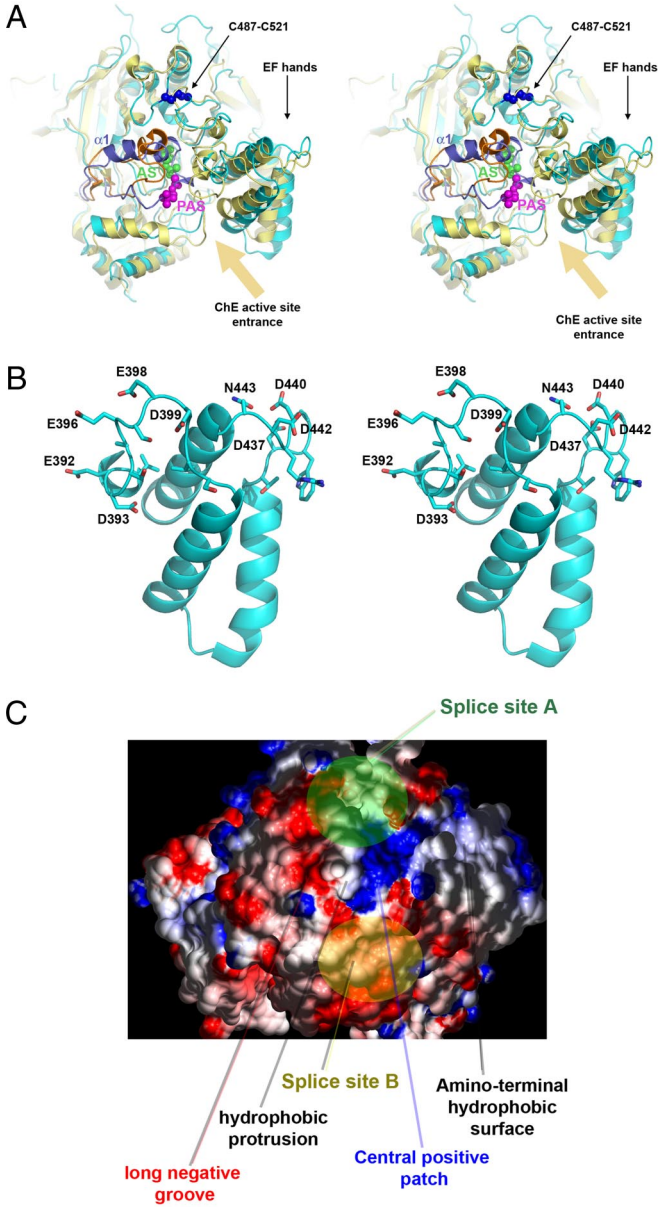


**Fig. 3.** Active-site occlusion and EF hands in the NL2A structure. (*A*) Superposition of mouse NL2A (cyan) and human AChE (PDB entry 2HA4) (yellow) shows that the deep active-site groove characteristic of AChEs is occluded in NL2A. The long omega loops are highlighted in dark blue and orange in NL2A and AChE, respectively. The C487–C521 disulfide bond, unique to and conserved among NLs, is shown as dark blue spheres. Acetylcholine molecules bound at the active site (AS) and peripheral anionic site (PAS) of AChE are shown as space-filling models in green and magenta, respectively. (*B*) Stereo diagram of the EF hand region. Side chains are shown for the loop regions of the EF hand helix–loop–helix motif. Potential $Ca^{2+}$ coordinating side chains are labeled. (*C*) Electrostatic surface of NL2 near the splice insertion sites. The surface is colored from blue to red for electrostatic potentials ranging between +5 and −5 *kT*. Positions of splice site A and B are shown as transparent yellow and green regions. Four prominent surface features near the alternative splice sites are conserved among NLs: a long negative groove, a central positive patch, a hydrophobic protrusion between them, and an amino terminal hydrophobic surface.

lack the two-stranded connecting $\beta$-sheet that holds EF hand pairs together in other structures, and the side chains of the putative $Ca^{2+}$ binding residues are oriented such that they could not coordinate a shared $Ca^{2+}$ ion without structural rearrangement. It thus appears unlikely that the absence of calcium is

BIOPHYSICS

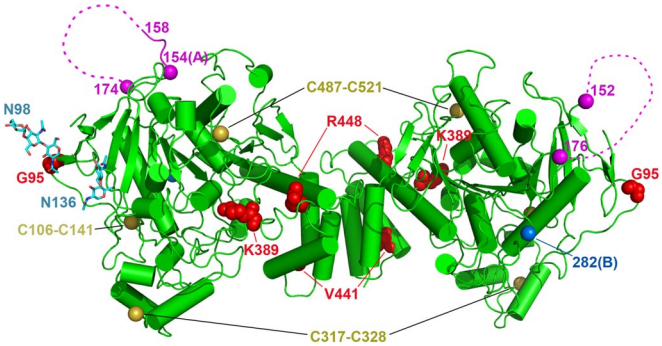


**Fig. 4.** NL mutants implicated in ASDs. Residues implicated in ASDs are shown in space-filling representation in red. Disulfide bonds are indicated by yellow spheres, and carbohydrate moieties are shown as stick models. The mapped positions of the B splice insertion sites are shown as blue spheres. The beginning and end points of the A splice insertion sites are shown as magenta spheres, and the path of the disordered A insertion sequences are shown as dotted lines.

solely attributable to detection limitations arising from the 3.3-Å diffraction limit of the NL2A crystals. These data suggest that the EF hand motif residues do not by themselves bind $Ca^{2+}$, and that the calcium dependence for NL-NRX interactions is unlikely to be due to calcium binding sites residing in NL alone. However, it remains possible that other interacting partners could be required for stabilization and coordination of calcium at the NL EF hand sites.

Analysis of sequence conservation highlights the C-terminal dimerization site, but no other sites have clearly demarcated patterns of conservation that might be indicative of functional significance. However, given that splice insertions of NL can affect binding to NRX, the predicted NRX binding site is expected to lie in close proximity to the A and B splice insertions of NL. The crystal structure of NL2A reveals that the A splice insertion, which encompasses residues 152–169, is positioned in the $\beta$6–$\beta$7 loop. The inserted sequence is mostly disordered in the structure; electron density is observed only for residues 152–158 in one protomer and is entirely absent in the other (Figs. 1 and 4). It remains to be shown whether this loop adopts a more rigid conformation upon interaction with NL2A ligands. Although the mouse NL2 gene does not encode a B splice insertion, the crystal structure allowed us to map the position of the B splice site according to sequence comparisons with NL1 (SI Fig. 5). This analysis predicts that the B insertion will form a short extended loop situated at the turn between the $\alpha$7-helix and $\beta$10-strand. Notably, this position is located on the same surface as the A splice insertion, suggesting that this region of the NL2 molecule likely represents the NRX binding interface.

Surface plasmon resonance studies show that NL-NRX binding affinity decreases with increasing ionic strength, implying that NL-NRX binding is at least in part based on electrostatic interactions (1). Therefore, we calculated the electrostatic potential (26) in the region of the candidate interaction surface. This analysis identified four distinct regions that could contribute to NRX-binding (Fig. 3*C*): (*i*) a large negative groove that transverses the distance between loop of splice site A and predicted splice site B, (*ii*) a large central positive patch between the positions of the splice insertion sites, (*iii*) a small hydrophobic protrusion between the charged patches, and (*iv*) a large conserved hydrophobic surface near the N terminus. Homology models for NL1 and NL3, built based on the NL2A structure, reveal that each of these four features is clearly conserved among NLs 1, 2, and 3. It is possible that one or several of these regions contain residues critical for binding presynaptic NRXs; however, this awaits further study.

## Discussion

Experimental evidence from cell biological and biochemical assays supports a role of the NL-NRX adhesion complex in bidirectionally orchestrating pre- and postsynaptic junction formation and/or maturation. However, the exact nature of specific NL and NRX variant interactions has not been elucidated. The crystal structure of the extracellular cholinesterase domain of NL2A reported here reveals important insights as to the molecular basis of NL-NRX interactions. NL2A forms a characteristic $\alpha/\beta$ hydrolase fold and exhibits an overall topology and structure very similar to ChE, including a similar dimerization interface and conserved EF hand motifs. However, there are clear structural differences that are related to the specific functions of the two proteins. In the following, we summarize these differences with an emphasis on those aspects of the NL2A structure that relate to its interactions with neurexins.

**ChE Active Site.** The active site of AChE is characterized by the presence of a Ser–His–Glu catalytic triad located at the base of a deep narrow gorge. The entrance to this active-site cleft is surrounded by negatively charged residues making up the PAS. Unlike ChEs, all NLs contain a glycine in place of the active-site serine and are therefore catalytically inactive. Further, the crystal structure of NL2A demonstrates that NLs also differ from ChEs in the active-site region by the presence of an omega loop, comprising residues 107–141, that occludes the active-site gorge and PAS binding site. This segment is characterized by high levels of sequence and size conservation that are distinct for the group of vertebrate NLs, invertebrate NLs, and ChEs, with significant differences between individual groups (SI Fig. 5). However, because the size of the insert in invertebrate NLs is much closer to that of vertebrate NLs than to ChEs, it is possible that the inserted sequences also play a similar occlusive role in the invertebrate molecules. However, stabilization of the omega loop within the active-site pocket by the Cys-487–521 disulfide bridge is unique in vertebrate NLs, suggesting that an alternate mechanism of stabilizing the omega loop might be used in invertebrates.

**Dimerization Interface.** Lateral clustering of NLs induces presynaptic NRX clustering and triggers the bidirectional nucleation of pre- and postsynaptic specialization. The structure of NL2A confirms that, as observed for AChE, the dimerization interface consists of a four-helix bundle with each monomer contributing two helices. Mutagenesis analysis revealed that residues at this dimerization interface are required for the ability of NL form homooligomers (10). Interestingly, the near complete conservation of dimer interface residues among NL isoforms (SI Fig. 5) leads to the possibility of heterodimerization. Immunoprecipitation from brain homogenates suggests that NL2 is associated in a complex with NL3 (19); however, it is not yet known whether this represents direct heterodimeric association between NL2 and NL3. The possibility of heterodimerization is intriguing because it could potentially allow NL isoforms to interact differentially with distinct presynaptic NRXs or other binding partners. Further study will be required to delineate these possibilities.

**EF Hand Regions.** Although the crystallization conditions contained 3 mM $Ca^{2+}$, which is ≈3-fold higher than the calcium concentration in the synaptic cleft, bound $Ca^{2+}$ ions were not detected in electron density maps of NL2A. This result is surprising in light of previous studies identifying NL but not NRX as the calcium binding molecule of the NL-NRX complex (2). Furthermore, previous modeling analyses suggested that NLs contain EF hand motifs and bind $Ca^{2+}$ via these conserved regions (25). In the structure of NL2A (Fig. 3*B*), we do observe helix–loop–helix motifs containing residues

with potential $Ca^{2+}$ binding side chains characteristic of EF hands. This raises the possibility that these $Ca^{2+}$ binding residues might require a NL binding partner for joint $Ca^{2+}$ coordination. Neurexins are not ideal candidates to bind at EF hands, however, because these regions are located at the opposite surface from the predicted NRX binding site. Because NRXs are the only known proteins to interact with the ChE domain of NLs, an alternate possibility is that a previously unidentified binding partner associates with NL at the EF hand sites and may aid the coordination of calcium ions.

The absence of bound $Ca^{2+}$ in the NL crystal structure, taken together with recent studies linking NRXs to $Ca^{2+}$ binding (24), supports the notion that NRXs, rather than NLs, might mediate the $Ca^{2+}$ binding required for NL-NRX adhesion. Crystallographic studies have identified bound $Ca^{2+}$ ions in crystal structures of LNS (laminin–neurexin–sex-hormone) domain 2 from $\alpha$-NRX1 (24). Recent studies from our own laboratory reveal a similar $Ca^{2+}$ binding site in the LNS6 domain, which encompasses the NL binding site in $\beta$-NRXs. Moreover, the NRX calcium binding residues are localized on the predicted NL binding surface in close proximity to the NRX splice site insertions and are thereby poised to contribute to interactions with binding partners. Additional evidence is provided by sequence analysis that reveals that $Ca^{2+}$ coordination at these sites may underlie a common mechanism for NRX binding interactions (24). Supporting this hypothesis, a recent mutagenesis analysis of the NRX extracellular domain demonstrated loss of NL binding and NRX function upon mutation of two of the putative calcium binding residues (27). Although these studies implicate NRXs in calcium-dependent binding, it remains possible that both NLs and NRXs, either individually or together, are involved in imparting the calcium dependence of the NL-NRX adhesive connection. However, cocrystal structures of NL in complex with NRX will be required to resolve this question.

**Sites of Alternative Splicing.** Alternative splicing in the extracellular domains of NL and NRX is thought to regulate adhesion between this pair of transsynaptic proteins. In the NL structure, both the A and B splice site insertions are predicted to form surface loops localized on the opposite face of the molecule from the region that corresponds to the AChE active site. Based on the critical role of the splice insertions in NRX binding, the surrounding regions are proposed to contain the NRX binding interface. The loops containing the A and B splice insertions are separated by between 15 and 30 Å. This close apposition is consistent with the possibility that a bound presynaptic NRX molecule could from simultaneous contacts with residues from both splice insertions. In the NL2A structure, the majority of the 17 residues inserted at the A site are disordered, making it difficult to predict the potential contribution of the A insert to NRX binding at this time. However, the splice insertion loops can be used to delineate the surface that may contain critical sites for NRX binding.

Because electrostatic interactions have been implicated in NL-NRX binding (1), we carried out calculations of electrostatic potential on NL2A and two homology models and identified four patches on the surface that are near splice sites A and B and, based on their conserved electrostatic features, appear to constitute likely sites for the NRX binding interface. These include a negative groove, a nearby positive region, and two nonpolar patches (Fig. 3*C*). The contribution of electrostatic forces to NRX binding has been demonstrated by a previous study that showed that mutation of charged residues flanking the B insert region in NL1 resulted in decreased NRX binding (22). Future studies employing mutational analysis will be required to pinpoint other residues critical for NRX binding and to confirm the assignment of this surface as the NRX binding interface.

**Mapping ASD Mutations to the Structure of NL2.** Mutations in NL3 and NL4 have recently been identified in a subset of human patients with ASDs (12–14). All of the identified mutations reside within the ChE domain; however, the cellular basis for functional deficits is not known. To gain insight into a potential structural basis for disrupted NL function, we mapped NL3 and NL4 ASD mutations onto the NL2 structure. These include the R451C (R448C in NL2) mutation in NL3, and G95S, K389R, and V414M (NL2A numbering) mutations in NL4 (14). At this time, only the NL3 R451C mutant has been characterized, and cellular assays implicate a protein trafficking defect for loss of function. The mutant NL3 is largely retained in the ER, but the ability of NL3 R451C to bind NRX and induce presynaptic terminals reaches normal levels if high levels of mutant protein are expressed (28, 29).This mutation appears to cause a significant disruption of neuronal circuit development because NL3 R451C knockin mice exhibit impaired social interactions, which is a phenotype reminiscent of human autism (30). In the structure of NL2A, R448 is located within the $\alpha$15-helix of the predicted EF hand region (Fig. 3*B*). This region is distal from the expected site of NRX interaction, which is consistent with normal NRX binding of R451C.

ASD-related NL4 mutations also localize to regions distant from the predicted NRX binding interface: K389R and V414M are localized near R451C in the region of the EF hand motif (Fig. 4), whereas Gly-95 is located at the tight turn immediately before the N-glycosylation site Asn-98. In overexpression analysis in neurons, NL2 G95S and NL2 K389R appear to maintain normal transport to the cell surface and induction of presynaptic vesicle clustering (E.C.B. and P.S., unpublished observation). Further analysis will be required to determine whether these mutations lead to defects in synapse function under other conditions. The localization of these mutated residues outside of the predicted NRX binding interface, taken together with the previously characterized NL3 R451C mutation, suggests that the NL mutations associated with ASD may interfere with crucial interactions of NLs other than their binding to presynaptic NRXs. However, mechanisms by which such interactions could lead to dysfunction are currently not clear.

## Materials and Methods

**Protein Expression and Purification.** Secondary structure prediction was used to approximate the ordered part of the extracellular domain of mouse neuroligin 2 with splice insertion A (residues 42–612). This region was fused to the endogenous signal sequence (residues 1–14) and a C-terminal 8× His-tag, cloned into pCEP4 vector (Invitrogen), and overexpressed in glycosylation-deficient HEK 293 cells. Spent medium was collected, and binding buffer was added to final concentrations of 500 mM NaCl, 20 mM Tris (pH 8.0), 20 mM imidazole (pH 8.0), and 3 mM $CaCl_2$. The medium was filtered through a 0.22-$\mu$m filter and passed over HisTrap HP columns (Amersham). The columns were washed with 500 mM NaCl, 20 mM Tris (pH 8.0), 20 mM imidazole (pH 8.0), and 3 mM $CaCl_2$, and the protein was eluted with 500 mM NaCl, 20 mM Tris (pH 8.0), 250 mM imidazole (pH 8.0), and 3 mM $CaCl_2$. The eluent was dialyzed against 100 mM NaCl, 20 mM Bis-Tris (pH 6.0), and 3 mM $CaCl_2$ at 4°C overnight and then applied to a Mono S column equilibrated with the same buffer. The flow-through was passed over a Mono Q equilibrated with the same buffer and eluted at 275 mM NaCl. Finally, the protein was subjected to size-exclusion chromatography (Superdex 200) in 150 mM NaCl, 10 mM Tris (pH 8.0), and 3 mM $CaCl_2$.

**X-Ray Data Collection, Structure Determination, and Analysis.** Diffraction data were collected on single crystals frozen at 100 K by using a cryoprotectant composed of mother liquor supplemented with 35% sucrose. The crystal structure of NL2A at 3.3-Å resolution was determined by multiple isomorphous replacement with anomalous scattering (MIR/AS) aided by molecular replacement, with solvent flattening and fourfold averaging. Two heavy atom derivatives, $K_2PtCl_6$ and $K_2HgI_4$, were identified by native gel screening (31) of NL2A. Their positions were determined by using phases from a poor molecular replacement solution obtained with an AChE domain search model from PDB entry 1POI, which shares 28% sequence identity with the NL2A AChE-like

domain. Because both of these derivatives showed good isomorphism statistics with the native crystals, MIR/AS calculations using the maximum-likelihood phasing program SHARP (32) were used to generate phases. Molecular transformations between the four molecules in the asymmetric unit were determined and used for resolution extension of the phases by solvent flattening and averaging. An excellent experimental map was obtained, and a model was built by using the CCP4 program Coot (33). Refinement proceeded with the programs CNS (34) and refmac (33), yielding a refined model with $R = 0.219$ and $R_{free} = 0.262$.

Homology models of NL1 and NL3 were built by using the NL2 structure as a template. The NL1 and NL3 sequences were first aligned to NL2 with T-COFFEE (35), and the resulting alignments were given as input to the NEST homology modeling program with default parameters (36). Electrostatic calculations were carried out with the program GRASP (26).

**ACKNOWLEDGMENTS.** This work was supported by National Institutes of Health Grants U54 CA121852 (to L.S.) and R01 NS045014 (to P.S.). E.C.B. was supported by National Research Service Award F30MH083473. B.H. is an investigator of the Howard Hughes Medical Institute. X-ray data were acquired at the X4A and X4C beamlines of the National Synchrotron Light Source, Brookhaven National Laboratory, which is operated by the New York Structural Biology Center.

1. Comoletti D, *et al.* (2003) Characterization of the interaction of a recombinant soluble neuroligin-1 with neurexin-1$\beta$. *J Biol Chem* 278:50497–50505.
2. Nguyen T, Sudhof TC (1997) Binding properties of neuroligin 1 and neurexin 1$\beta$ reveal function as heterophilic cell adhesion molecules. *J Biol Chem* 272:26032–26039.
3. Boucard AA, Chubykin AA, Comoletti D, Taylor P, Sudhof TC (2005) A splice code for trans-synaptic cell adhesion mediated by binding of neuroligin 1 to $\alpha$- and $\beta$-neurexins. *Neuron* 48:229–236.
4. Ichtchenko K, *et al.* (1995) Neuroligin 1: A splice site-specific ligand for $\beta$-neurexins. *Cell* 81:435–443.
5. Ichtchenko K, Nguyen T, Sudhof TC (1996) Structures, alternative splicing, and neurexin binding of multiple neuroligins. *J Biol Chem* 271:2676–2682.
6. Missler M, Fernandez-Chacon R, Sudhof TC (1998) The making of neurexins. *J Neurochem* 71:1339–1347.
7. Chubykin AA, *et al.* (2005) Dissection of synapse induction by neuroligins: Effect of a neuroligin mutation associated with autism. *J Biol Chem* 280:22365–22374.
8. Varoqueaux F, *et al.* (2006) Neuroligins determine synapse maturation and function. *Neuron* 51:741–754.
9. Chubykin AA, *et al.* (2007) Activity-dependent validation of excitatory versus inhibitory synapses by neuroligin-1 versus neuroligin-2. *Neuron* 54:919–931.
10. Dean C, *et al.* (2003) Neurexin mediates the assembly of presynaptic terminals. *Nat Neurosci* 6:708–716.
11. Graf ER, Zhang X, Jin SX, Linhoff MW, Craig AM (2004) Neurexins induce differentiation of GABA and glutamate postsynaptic specializations via neuroligins. *Cell* 119:1013–1026.
12. Jamain S, *et al.* (2003) Mutations of the X-linked genes encoding neuroligins NLGN3 and NLGN4 are associated with autism. *Nat Genet* 34:27–29.
13. Laumonnier F, *et al.* (2004) X-linked mental retardation and autism are associated with a mutation in the NLGN4 gene, a member of the neuroligin family. *Am J Hum Genet* 74:552–557.
14. Yan J, *et al.* (2005) Analysis of the neuroligin 3 and 4 genes in autism and other neuropsychiatric patients. *Mol Psychiatry* 10:329–332.
15. Changeux JP (1966) Responses of acetylcholinesterase from *Torpedo marmorata* to salts and curarizing drugs. *Mol Pharmacol* 2:369–392.
16. Grifman M, Galyam N, Seidman S, Soreq H (1998) Functional redundancy of acetylcholinesterase and neuroligin in mammalian neuritogenesis. *Proc Natl Acad Sci USA* 95:13935–13940.
17. Chih B, Engelman H, Scheiffele P (2005) Control of excitatory and inhibitory synapse formation by neuroligins. *Science* 307:1324–1328.
18. Scheiffele P, Fan J, Choih J, Fetter R, Serafini T (2000) Neuroligin expressed in nonneuronal cells triggers presynaptic development in contacting axons. *Cell* 101:657–669.
19. Budreck EC, Scheiffele P (2007) Neuroligin-3 is a neuronal adhesion protein at GABAergic and glutamatergic synapses. *Eur J Neurosci* 26:1738–1748.
20. Song JY, Ichtchenko K, Sudhof TC, Brose N (1999) Neuroligin 1 is a postsynaptic cell-adhesion molecule of excitatory synapses. *Proc Natl Acad Sci USA* 96:1100–1105.
21. Varoqueaux F, Jamain S, Brose N (2004) Neuroligin 2 is exclusively localized to inhibitory synapses. *Eur J Cell Biol* 83:449–456.
22. Comoletti D, *et al.* (2006) Gene selection, alternative splicing, and post-translational processing regulate neuroligin selectivity for $\beta$-neurexins. *Biochemistry* 45:12816–12827.
23. Chih B, Gollan L, Scheiffele P (2006) Alternative splicing controls selective trans-synaptic interactions of the neuroligin-neurexin complex. *Neuron* 51:171–178.
24. Sheckler LR, Henry L, Sugita S, Sudhof TC, Rudenko G (2006) Crystal structure of the second LNS/LG domain from neurexin 1$\alpha$: $Ca^{2+}$ binding and the effects of alternative splicing. *J Biol Chem* 281:22896–22905.
25. Tsigelny I, Shindyalov IN, Bourne PE, Sudhof TC, Taylor P (2000) Common EF-hand motifs in cholinesterases and neuroligins suggest a role for $Ca^{2+}$ binding in cell surface associations. *Protein Sci* 9:180–185.
26. Petrey D, Honig B (2003) GRASP2: Visualization, surface properties, and electrostatics of macromolecular structures and sequences. *Methods Enzymol* 374:492–509.
27. Graf ER, Kang Y, Hauner AM, Craig AM (2006) Structure function and splice site analysis of the synaptogenic activity of the neurexin-1$\beta$ LNS domain. *J Neurosci* 26:4256–4265.
28. Chih B, Afridi SK, Clark L, Scheiffele P (2004) Disorder-associated mutations lead to functional inactivation of neuroligins. *Hum Mol Genet* 13:1471–1477.
29. Comoletti D, *et al.* (2004) The Arg451Cys-neuroligin-3 mutation associated with autism reveals a defect in protein processing. *J Neurosci* 24:4889–4893.
30. Tabuchi K, *et al.* (2007) A neuroligin-3 mutation implicated in autism increases inhibitory synaptic transmission in mice. *Science* 318:71–76.
31. Boggon TJ, Shapiro L (2000) Screening for phasing atoms in protein crystallography. *Structure* 8:R143–R149.
32. Bricogne G, Vonrhein C, Flensburg C, Schiltz M, Paciorek W (2003) Generation, representation and flow of phase information in structure determination: Recent developments in and around SHARP 2.0. *Acta Crystallogr D* 59:2023–2030.
33. The CCP4 Consortium (1994) The CCP4 suite: Programs for protein crystallography. *Acta Crystallogr D* 50:760–763.
34. Brunger AT, *et al.* (1998) Crystallography & NMR system: A new software suite for macromolecular structure determination. *Acta Crystallogr D* 54:905–921.
35. Notredame C, Higgins DG, Heringa J (2000) T-Coffee: A novel method for fast and accurate multiple sequence alignment. *J Mol Biol* 302:205–217.
36. Petrey D, *et al.* (2003) Using multiple structure alignments, fast model building, and energetic analysis in fold recognition and homology modeling. *Proteins* 53(Suppl 6): 430–435.